Catalysis Science & Technology

Accepted Manuscript

ROYAL SOCIETY OF CHEMISTRY

www.rsc.org/catalysis

Journal Name

ARTICLE

Identification of the reaction pathway and reactive species of the selective catalytic reduction of NO with NH_3 over cerium-niobium oxide catalysts

Received 00th January 20xx,
Accepted 00th January 20xx

DOI: 10.1039/x0xx00000x

www.rsc.org/

Ruiyang Qu,[a, b] Yue Peng,[a] Xiaoxu Sun,[a] Junhua Li,[*a] Xiang Gao,[*b] and Kefa Cen[b]

A series of Ce-Nb oxide catalysts were synthesized with different calcination temperatures for the selective catalytic reduction (SCR) of NO with NH_3 and we investigated the reaction pathway and reactive species in detail. The SCR reaction pathway over the Ce-Nb catalysts followed both Eley–Rideal mechanism and Langmuir–Hinshelwood mechanism, where the former contributed more especially at high reaction temperatures. Lewis acidity was found to be catalytically important in the Eley–Rideal mechanism. NO_2 and monodentate nitrate were the main reactive species in the Langmuir–Hinshelwood mechanism. The catalyst calcined at lower temperatures exhibited higher catalytic activity at low temperatures but lower activity at high temperatures. With the increase of calcination temperature, the catalyst surface was gradually covered by niobium oxide species, resulting in the enhancement of total acidity but the decline of redox ability, along with the decrease of the contribution of the Langmuir–Hinshelwood mechanism to the SCR reaction.

Introduction

Nitrogen oxides (NO_x), emitted from industrial combustion of fossil fuels and automobile exhaust gas, are major air pollutants. The selective catalytic reduction (SCR) of NO_x with ammonia as a reducing agent was considered as one of the most efficient technology for NO_x removal.[1] V_2O_5-WO_3(MoO_3)/TiO_2 catalyst has been industrialized for removing NO_x from stationary sources. But several problems still existed during the applications of the catalysts, such as: the relatively narrow operation temperature window, the high oxidation ratio of SO_2 to SO_3,[2] and the formation of N_2O at relatively high temperatures.[3]

For the reasons above, there have been many efforts in developing vanadium-free catalysts. Ceria-based catalysts[4-7] were extensively explored due to the high oxygen mobility and good redox properties of cerium oxide. Our groups have recently developed a novel Ce-Nb oxide catalyst for the SCR of NO with NH_3, and established the correlations among the structures, acid properties and redox behaviors of the catalyst.[8] This newly developed catalyst exhibited good catalytic activity in a wide temperature range from 200 to 450 $^{\circ}C$ as well as good water resistance, making it a promising catalyst for the industrial application. However, the reaction pathway and the reactive species over this novel catalyst are still not well understood, e.g. the contribution of Eley–Rideal (E-R) mechanism and Langmuir–Hinshelwood (L-H) mechanism to the SCR reaction, the reactive ad-NH_3 species (NH_4^+ linked to Brønsted acid site or NH_3 coordinated on Lewis acid site). Eley–Rideal mechanism was thought to dominate in the SCR reaction for vanadia-based catalysts due to the weak interaction between NO and the fully oxidized catalyst surfaces.[1] But other oxides, such as MnO_x-,[9] Fe_2O_3-,[10] CuO-,[11] and CeO_2-based catalysts,[12] preferred to strongly adsorb NO and Langmuir–Hinshelwood mechanism also contributed to the SCR reaction over these catalysts. Moreover, Topsøe[13] found a good correlation between the concentration of Brønsted acid sites and the NO_x conversion, thus regarding Brønsted acid sites as the catalytically important NH_3 adsorption sites. However, some catalysts without any Brønsted acidity prepared Ramis and his coworkers[11] also exhibited good low-temperature catalytic activity.

Identifying the reaction mechanism and the active sites is crucial for the practical application and the rational design and improvement of the catalyst. Based on our previous investigation,[8] we herein further explored the reaction pathway and the reactive species as well as calculating each contribution of Eley–Rideal mechanism and Langmuir–Hinshelwood mechanism to the SCR reaction using the catalysts with different calcination temperatures. Various characterization techniques including N_2 adsorption, X-ray diffraction (XRD), X-ray photoelectron spectroscopy (XPS), ammonia and NO_x temperature programmed desorption (NH_3-TPD and NO_x-TPD),

[a] State Key Joint Laboratory of Environment Simulation and Pollution Control, School of Environment, Tsinghua University, Beijing 100084, P. R. China. Email: lijunhua@tsinghua.edu.cn
[b] State Key Laboratory of Clean Energy Utilization, College of Energy Engineering, Zhejiang University, Hangzhou 310027, P. R. China. Email: xgao1@zju.edu.cn

hydrogen temperature programmed reduction (H_2-TPR) and in situ diffuse reflectance Fourier transform spectroscopy (*in situ* DRIFTS) were used to investigate the mechanistic aspects as well as the structures and physicochemical properties of the catalysts.

Experimental

Catalyst preparation

The Ce-Nb mixed oxides were synthesized using co-precipitation method, as described in previous study.[8] Typically, desired amount of cerium nitrate was dissolved in deionized water and niobium chloride in methanol, respectively. The molar ratio of Ce/Nb=1. These two solutions were mixed together, then added into an excess of ammonia solution with continuous stirring. The precipitates were collected by filtration for several times until no residue Cl- (detected by $AgNO_3$ solution), dried at 120 °C overnight and calcined at 500, 550, 600, or 700 °C for 5 h under static air conditions. The catalysts were denoted as CN500, CN550, CN600 and CN700, respectively. These catalysts were then crushed and sieved to 40~60 meshes for activity measurements.

Catalytic performance tests

The catalytic performance tests were performed in a fixed-bed quartz reactor (inner diameter 9 mm), using 0.1 or 0.02 g of catalyst (40~60 mesh). The feed gas mixture contained 500 ppm NO, 500 ppm NH_3, 5% O_2 and the balance of N_2. The total flow rate of the feed gas was 200 mL min-1, corresponding to a gas hourly space velocity (GHSV) of 120, 000 or 600, 000 mL g^{-1} h^{-1}. The concentrations of the outlet gases were continuously monitored by an FTIR spectrometer (MKS, MultiGas 2030HS). The experimental data were recorded only when the steady-state reaction was reached after 30 min at each temperature. NO conversion (X) is calculated as follows:

$$X = (1 - [\mathrm{NO}]_{\mathrm{out}}/[\mathrm{NO}]_{\mathrm{in}}) \times 100\% \quad (1)$$

where $[NO]_{in}$ and $[NO]_{out}$ represented the inlet and outlet concentrations of NO, respectively.

Catalyst characterizations

N_2 adsorption-desorption experiments were carried out using a Quantachrome Autosorb-1 instrument at -196 °C. The samples were degassed at 300 °C for 4 h before N_2 adsorption. The specific surface areas (SSA) were calculated by the Brunauer–Emmett–Teller (BET) equation at P/P_0 in the range from 0.05 to 0.35.

Powder X-ray diffraction (XRD) patterns were performed on an X-ray diffractometer (Rigaku, D/max-2200, Japan) with a Cu Kα radiation source (λ=0.15405 nm, 40 mV and 200 mA). The scanning range was between 10 and 80° at a step rate of 10° min-1 with the step size of 0.02°.

X-ray photoelectron spectroscopy (XPS) analysis was carried out on an ESCALab220i-XL electron spectrometer from VG Scientific using 300 W Mg Ka radiation. The base pressure was approximately 3×10^{-9} mbar. The binding energies of all the elements were referenced to the C 1s line at 284.8 eV from carbon impurities.

Temperature programmed desorption of ammonia and NO_x (NH_3-TPD and NO_x-TPD) was performed on an Chemisorb 2007 TPx using FTIR spectrometer (MKS, MultiGas 2030HS) for measuring different nitrogen-containing species (NH_3, N_2O and NO). The catalysts were pretreated at 350 °C for 1 h before the experiment. Then the samples were cooled down to 100 °C and saturated with NH_3 or NO+O_2, followed by flushing with N_2. Then the saturated catalysts were heated from 100 °C to 500 °C at a rate of 10 °C min^{-1}.

Temperature programmed reduction of hydrogen (H_2-TPR) was performed on a chemisorption analyzer (Micromeritics, ChemiSorb 2720 TPx). The catalysts were pretreated at 350 °C for 1 h before each experiment. The catalysts were then cooled down to room temperature in a flow of Ar. The reduction of the samples started from room temperature to 1000 °C, with a mixture of 5 % H_2/Ar (50 mL min^{-1}) at a heating rate of 10 °C min^{-1}. When calculating the activation energy of reduction, we set the heating rate=5, 10 and 20 °C min^{-1}. The consumption of H_2 was continuously monitored using a thermal conductivity detector (TCD).

In situ diffuse reflectance infrared Fourier transform spectroscopy (*in situ* DRIFTS) experiments were performed on an Fourier transform infrared spectrometer (FTIR, Nicolet NEXUS 6700), equipped with an MCT/A detector. The catalysts were pretreated at 350 °C for 1 h in N_2 with a flow of 100 mL min^{-1} before each experiment. All the IR spectra were recorded by collecting 32 scans with a resolution of 4 cm^{-1}.

Results

Catalytic activity tests. The catalytic performances of the catalysts with different calcination temperatures are shown in Fig. 1. All the catalysts exhibited good catalytic activities from 300 to 400 °C. However, remarkable differences are observed at low temperatures, especially from 150 °C to 200 °C. The catalyst calcined at 500 °C (CN500) showed the best NO reduction performance in the temperature range. In addition, the higher the calcination temperature, the lower the catalytic activities in this temperature range. Considering the fact that

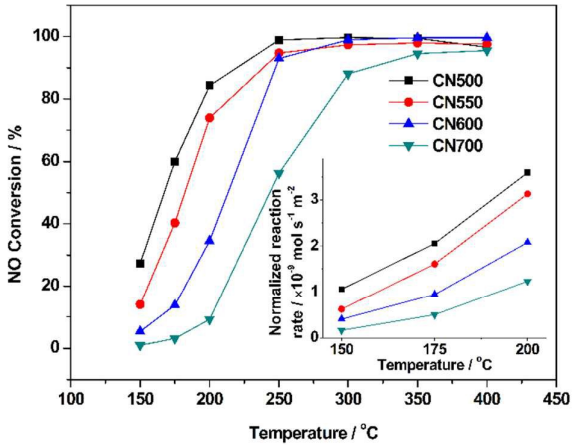

different calcination

Fig. 1. SCR performances over Ce-Nb oxide catalysts with different calcination temperatures. Reaction condition: [NH_3]=[NO]=500 ppm, [O_2]=5 %, total flow rate=200 mL min^{-1}, catalyst mass=0.1 g, 0.02 g (inset) GHSV=120, 000 mL g^{-1} h^{-1}, 600, 000 mL g^{-1} h^{-1} (inset).

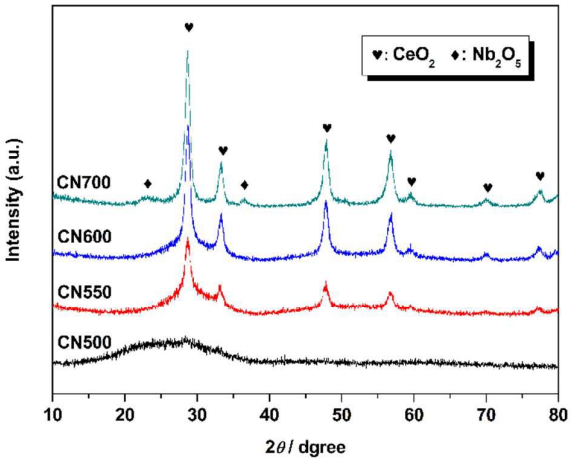

Fig. 2. XRD patterns of the Ce-Nb oxide catalysts with different calcination temperatures.

temperatures may affect the specific surface areas (S_{BET}) of the catalysts, which leads to the differences in the apparent catalytic activities, we normalized the reaction rates in the temperature range from 150 °C to 200 °C by S_{BET} in order to eliminate the influence of S_{BET}. Herein a higher GHSV (600, 000 mL g^{-1} h^{-1}) was used to decrease the conversions, which could help to avoid diffusion limited conditions. As shown in the inset of Fig. 1, similar results are also obtained.

X-ray diffraction (XRD). The crystallization of the catalysts was determined by XRD and the results are shown in Fig. 2. With respect to CN500, no diffraction peaks are observed, suggesting an amorphous structure. As for the catalysts calcined at 550 and 600 °C, we can see typical diffraction patterns for cerium oxide (PDF-ICDD 65-2975). As for CN700, peaks for not only cerium oxide but also niobium oxide was obtained. Moreover, the peaks for CeO_2 became sharper with increasing calcination temperature, it indicates that better crystallization was happened.

X-ray photoelectron spectroscopy (XPS). The concentrations of surface elements were determined by XPS technique. The concentration ratios of Nb/Ce are listed in Table 1. Obviously, the relative concentration of niobium enhanced with the increase of the calcination temperature, suggesting that niobium oxide species gradually covered the surface of the catalyst when the calcination temperature increased.

Table 1

The properties of the Ce-Nb oxide catalysts calcined at different temperatures

Sample	S_{BET} / m^2 g^{-1}	Nb/Ce
CN500	123	1.50
CN550	108	1.93
CN600	62	2.11
CN700	26	2.25

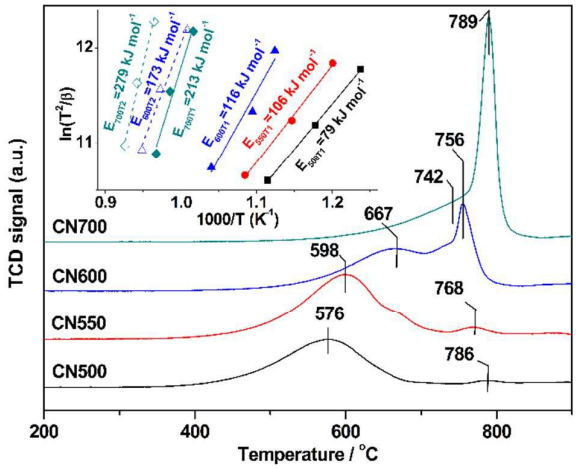

Fig. 3. H_2-TPR profiles of the Ce-Nb oxide catalysts with different calcination temperatures.

Temperature programmed reduction of hydrogen (H_2-TPR). The H_2-TPR was carried out to determine the redox properties of the catalysts, and the results are shown in Fig. 3. Both CN500 and CN550 had a major peak before 700 °C and a very weak peak after 700 °C, while CN600 and CN700 had two partially overlapped peaks. Considering the first peak (denoted as T1) for all the four samples, which is always regarded as the reduction of surface active oxygen,[14] we can easily observe that the temperatures of the reduction peak centers follow the order: CN500 < CN550 < CN600 < CN700. The second reduction peak (denoted as T2) was due to the reduction of bulk oxygen.[14] In order to obtain further information on the kinetics, we calculated the apparent activation energy of reduction of the catalysts by altering the heating ramp (5, 10, 20 K min^{-1}). The results are summarized in the inset of Fig. 3. The apparent activation energies of the reduction process of different catalysts follow the same order as the above mentioned peak position. In addition, it should be noted that the apparent energy of the first peak of CN700 was even larger than that of the second peak of CN600, implying that the oxygen species in CN700 was much less reactive.

NO oxidation tests. The oxidation ability of NO with O_2 over the catalysts was tested and the results are shown in Fig. 4. In the whole temperature range, the NO conversion followed the order: CN500 > CN550 > CN600 > CN700. This result is in good accordance with the H_2-TPR results. The shift of the first reduction peak towards higher temperatures and the increment of activation energy of reduction implied that the surface oxygen became less reactive when the catalyst was calcined at higher temperatures, thus leading to the decline of NO oxidation ability.

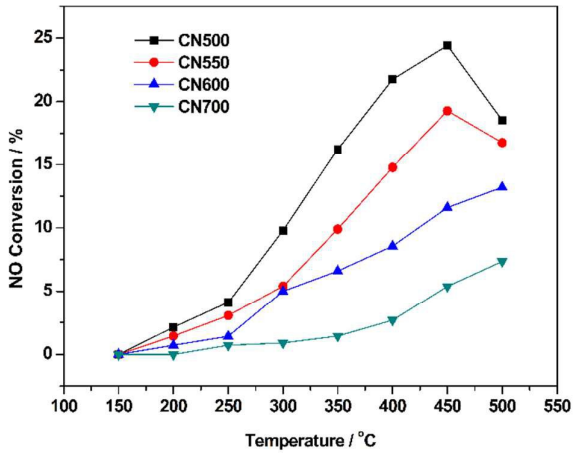

Fig. 4. NO oxidation with O_2 over the Ce-Nb oxide catalysts with different calcination temperatures. Reaction condition: [NO]=500 ppm, [O_2]=5 %, total flow rate=200 mL min^{-1}, catalyst mass=0.1 g.

***In situ* diffuse reflectance infrared Fourier transform spectroscopy (*in situ* DRIFTS).** (1) NH_3 adsorption. We carried out *in situ* DRIFTS of NH_3 adsorption at 100 °C to illustrate the surface acid sites on these catalysts and the results are shown in Fig. 5. In Fig. 5(a), the bands centered at 1169, 1173 and 1206 cm^{-1} are assigned to the symmetric bending vibration of coordinated NH_3 on Lewis acid site.[12] The ones at 1433 cm^{-1} are attributed to the asymmetric bending vibration of NH_4^+ species on Brønsted acid site.[12] In each catalyst, these two peaks were selected as the representative peaks for NH_3 adsorbed on Lewis and Brønsted acid sites due to their relatively strong intensities. It can be easily observed that both Brønsted and Lewis acid sites are presented on the surfaces of the catalysts. However, considering the relative intensities of the bands, we can find

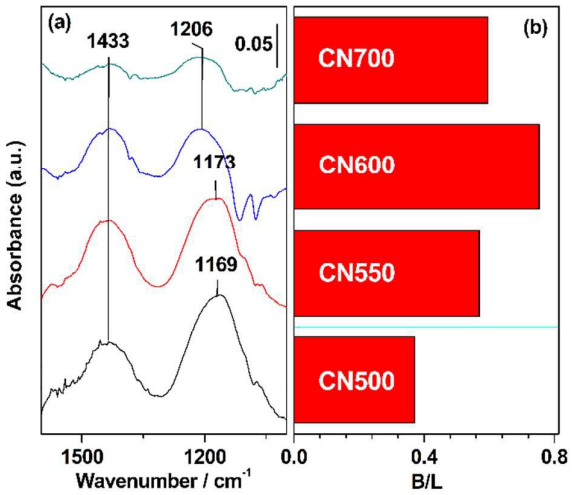

Fig. 5. (a) *In situ* DRIFTS of NH_3 adsorption at 100 °C over the Ce-Nb oxide catalysts with different calcination temperatures. (b) Ratio of the number of Brønsted acid sites to the number of Lewis acid sites.

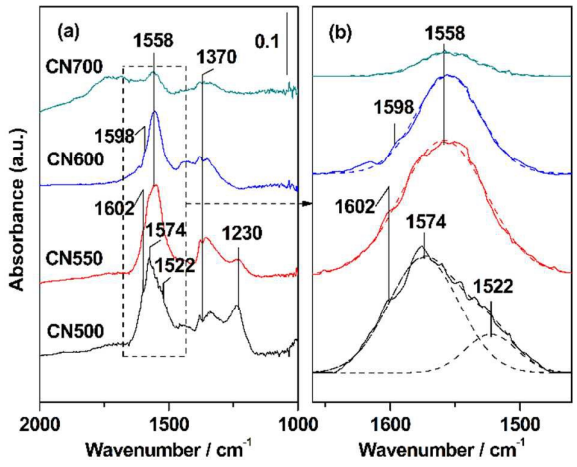

Fig. 6. (a) *In situ* DRIFTS of adsorbed NO+O_2 at 200 °C over the Ce-Nb oxide catalysts with different calcination temperatures. (b) The amplification of the selected field of (a).

some differences. The ratio of Brønsted acid sites to Lewis acid sites by integrating these two bands, denoted as B/L, was used to indicate the distribution of surface acid sites, and the results are shown in Fig. 5(b). The B/L ratio follows the order CN500 < CN550 < CN600, but CN700 < CN600. The former trend is related to the different coverages of niobium oxide species on the catalyst surfaces, which is consistent with our previous study.[8] The later trend may be due to the formation of bulk niobium oxides species on CN700, as is evidenced by XRD results.

(2) NO+O_2 adsorption. *In situ* DRIDTS of NO+O_2 coadsorption at 200 °C was performed to determine the surface nitrate/nitrite species during the reaction process and the results are shown in Fig. 6. When saturated with NO+O_2, the catalyst surfaces were dominantly covered by nitrate species, as shown in Fig. 6(a). Bands at 1230 cm^{-1} were ascribed to bridging nitrate.[10,15,16] The bands at 1370 cm^{-1} could be assigned to nitro compounds.[15] The band at 1522 cm^{-1} can be attributed to the monodentate nitrate.[15,17] The bands at 1574 and 1558 cm^{-1} were assigned to bidentate nitrate.[15,18] The assignments of the bands at 1598 and 1602 cm^{-1} varied in previous studies by different researchers. Liu and his coworkers[10] ascribed these bands to bridging nitrates, along with the bands at 1230 cm^{-1}. But in our study, as shown in Fig. 6(b), the catalyst CN600 exhibited a small shoulder at 1598 cm^{-1} and no bands at around 1230 cm^{-1}. So we attributed this band to the asymmetric frequency of NO_2 species, as discussed by previous researchers.[12,19] While the peak at 1602 cm^{-1} over CN500 and CN550 was due to the overlap of NO_2 and bridging nitrate. Magnifying the region of 1660 to 1460 cm^{-1}, as shown in Fig. 6(b), we can see that CN500 had two overlapped peaks and a small shoulder, while CN550, CN600 and CN700 only presented one main peak. This result suggests that monodentate nitrate existed only on the surface of CN500.

(3) Transient reactions. *In situ* DRIFTS of transient reactions at 200 °C was also carried out to explore the reaction mechanism. The catalyst CN500 was selected to evaluate. In Fig. 7(a), the catalyst surface was first saturated with NH_3, and then passed

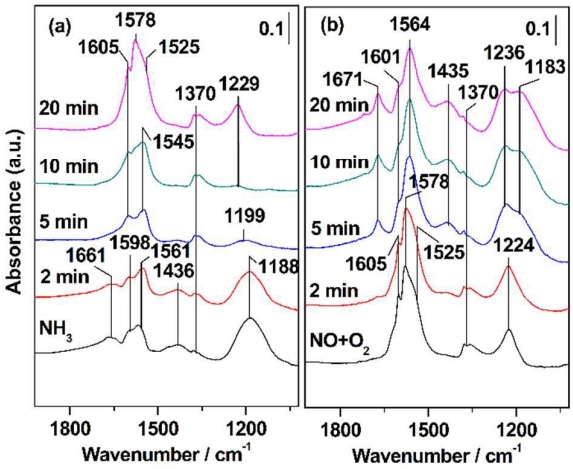

Fig. 7. *In situ* DRIFTS of (a) adsorbed NH_3 reacting with gaseous NO and O_2; (b) adsorbed $NO+O_2$ reacting with gaseous NH_3.

over by $NO+O_2$. The bands at 1188 and 1598 cm^{-1} are ascribed to the symmetric and asymmetric bending vibrations of coordinated NH_3 species on Lewis acid site,[12] and the bands at 1436 and 1661 cm^{-1} to the asymmetric and symmetric bending vibrations of NH_4^+ species on Brønsted acid site.[12] The bands at 1370 and 1561 cm^{-1} were likely attributed to the oxidized products of NH_3 by the catalyst. $NO+O_2$ were then introduced to the IR cell. After 5 minutes, the adsorbed NH_3 species, both on Lewis and Brønsted acid site, were totally consumed. Meanwhile, some bands attributed to monodentate, bidentate and bridging nitrate species appeared. After 20 minutes, the catalyst surface were covered with these nitrate species, similar to the results of $NO+O_2$ adsorption on the catalyst surface as shown in Fig. 6. Then the catalyst was purged by N_2 for 15 minutes. NH_3 was reversely introduced into the cell to see how the adsorbed nitrate species reacted with NH_3. After 5 minutes, the peak for gaseous NO_2 at 1605 cm^{-1} and monodentate nitrate at 1525 cm^{-1} diminished, at the same time the bands for ad-NH_3 species at 1183, 1433, 1601 and 1671 cm^{-1} appeared. Meanwhile the peak for bidentate nitrate at 1578 cm^{-1} shifted to 1564 cm^{-1} and the one for bridging nitrate at 1224 cm^{-1} shifted to 1236 cm^{-1}. Mass spectrometer (MS) was used to detect the product as N_2 cannot be detected by IR. The signals of N_2 (m/z=28) were found in both cases, confirming that the disappearance of the peaks was due to the reaction.

Discussions

Reaction mechanism over Ce-Nb oxide catalyst. The results of in situ DRIFTS study, as shown in Fig. 7 (a) and (b), reveal that both Eley–Rideal mechanism (E-R) and Langmuir–Hinshelwood mechanism (L-H) could occur during the reaction. The SCR reaction over E-R mechanism can be approximately described as:[1,20]

$$NH_3(g) \rightarrow NH_3(a) \quad (2)$$

$$NH_3(a) + Ce^{4+}_{surf} \rightarrow -NH_2 + Ce^{3+}_{surf} + H^+ \quad (3)$$

$$-NH_2 + NO(g) \rightarrow N_2 + H_2O \quad (4)$$

$$Ce^{3+}_{surf} + H^+ + 1/4\,O_2 \rightarrow Ce^{4+}_{surf} + 1/2\,H_2O \quad (5)$$

In Fig. 7(b), NO_2 could be involved in the reaction. Therefore the so-called "fast SCR" reaction[21] is likely to occur, which is always responsible for the low-temperature catalytic activity. This reaction pathway is depicted as follows:[12,21]

$$NH_3(g) \rightarrow NH_3(a) \quad (2)$$

$$1/2\,O_2(g) + \square \rightarrow O - \square \quad (6)$$

$$NO + O - \square \rightarrow -NO_2(a) \quad (7)$$

$$2NH_3(a) + NO + -NO_2(a) \rightarrow 2N_2 + 3H_2O \quad (8)$$

In Fig. 7(b), it also should be noted that the peak of monodentate nitrate diminished and the peaks of bidentate and bridging nitrates shifted after NH_3 passing over the NO_x-saturated catalyst for 5 minutes. These results suggest that bidentate and bridging nitrates could adsorb NH_3 species, thus leading to the shift of the characteristic bands, described as eq. (8)~(11).[22] But these two kinds of ammonium nitrates remained stable and did not involve in the reaction at 200 °C due to the relatively high thermal stability of bidentate and bridging nitrates.

$$NO(g) + Ce^{4+}_{surf} = O + 1/2\,O_2 \rightarrow Ce^{3+}_{surf} = (O_2) = NO\ \text{(bidentate nitrate)} \quad (9)$$

$$NO(g) + 2Ce^{4+}_{surf} = O \rightarrow Ce^{3+}_{surf} - O - (NO) - O - Ce^{3+}_{surf}\ \text{(bridging nitrate)} \quad (10)$$

$$NH_3(g) + Ce^{3+}_{surf} = (O_2) = NO \rightarrow Ce^{3+}_{surf} = (O_2) = NO - NH_3 \quad (11)$$

$$NH_3(g) + Ce^{3+}_{surf} - O - (NO) - O - Ce^{3+}_{surf} \rightarrow Ce^{3+}_{surf} - O - (NO - NH_3) - O - Ce^{3+}_{surf} \quad (12)$$

Unlike bidentate and bridging nitrates, monodentate nitrate could involve in the reaction. Similar result was also obtained previously by Liu and his coworkers.[10] The "nitrate route"[23,24] was found to dramatically enhance the low-temperature catalytic activity. Therefore, after ammonia attacking the monodentate nitrate species, the newly formed ammonium nitrate was easy to involve in the reaction due to the low stability of monodentate nitrate. The reaction pathway can be described as:[24]

$$NH_3(g) + Nb^{5+}_{surf} - OH \rightarrow Nb^{5+}_{surf} - O \cdots H - NH_3 \quad (13)$$

$$NO(g) + Ce^{4+}_{surf} = O + 1/2\,O_2 \rightarrow Ce^{3+}_{surf} - O - NO_2 \quad (14)$$

$$Ce^{3+}_{surf} - O - NO_2 + Nb^{5+}_{surf} - O \cdots H - NH_3 \rightarrow Nb^{5+}_{surf} - O \cdots NH_4NO_3 - Ce^{3+}_{surf} \quad (15)$$

$$Nb^{5+}_{surf} - O \cdots NH_4NO_3 - Ce^{3+}_{surf} + 2NO + 2NH_3 \rightarrow 3N_2 + 4H_2O + Nb^{5+}_{surf} - OH + Ce^{3+}_{surf} - OH \quad (16)$$

$$Ce^{3+}_{surf} - OH + 1/4\,O_2 \rightarrow Ce^{4+}_{surf} = O + 1/2\,H_2O \quad (17)$$

We calculated the contribution of E-R and L-H mechanisms to the reaction using the method proposed by our group in previous study.[25] Since the NO conversion was too high at temperatures above 200 °C, as shown in Fig. 1, we reduced the amount of the catalyst (20 mg) to enlarge the GHSV (600, 000 mL g^{-1} h^{-1}). The gas flow rate remained unchanged (200 mL

min^{-1}). By varying the gas concentrations, ([NH_3]=[NO]=500, 1000, 1500 ppm, [O_2]=5%, N_2 balanced, see SI) we calculated the reaction rate normalized by S_{BET} and the contribution of E-R and L-H mechanisms to the reaction, as shown in Fig. 8. Using the ratio of $C_{L\text{-}H}/(C_{E\text{-}R}+ C_{L\text{-}H})$ we could find that the contribution of the reaction rate through L-H mechanism gradually decreased with the increase of reaction temperature. This result is also in accordance with the previous study.[25] With the increase of

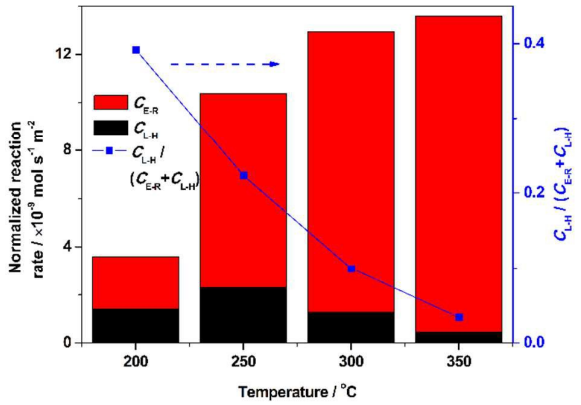

Fig. 8. Contribution of the Eley-Rideal mechanism and the Langmuir-Hinshelwood mechanism to the SCR reaction over CN500 catalyst. Reaction condition: [NH_3]=[NO]=500 ppm, [O_2]=5 %, total flow rate=200 mL min^{-1}, catalyst mass=0.02 g, GHSV=600, 000 mL g^{-1} h^{-1}.

temperature, the activation of NH_3, i.e. reaction (2), which is also regarded as the rate determining step of the E-R type mechanism,[1] is easier to happen. So the E-R mechanism accounts more for the SCR reaction at higher temperatures.

The acid property of the catalyst is also regarded as one of the key factors for the SCR reaction. There is still no unanimous consensus on whether the Lewis acid site or Brønsted acid site is more catalytically important. In our study, both Brønsted acid site and Lewis acid site could involve in the reaction, as shown in Fig. 7(a). But considering the number of Brønsted acid sites and Lewis acid sites, as determined by the peak intensities in Fig. 7(a), we can find that the number of Lewis acid sites was much larger than that of Brønsted acid sites. In addition, when the temperature increased, NH_4^+ bonded to Brønsted acid site quickly diminished and NH_3 coordinated to Lewis acid site still remained.[8] And the contribution of E-R mechanism became dominant at high temperatures, as shown in Fig 8. So we considered that Lewis acidity was catalytically more important in E-R mechanism, as shown in eq. (2) ~ (5).

Effect of calcination temperature. The differences in calcination temperatures resulted in the variations of catalyst structures and the physiochemical properties, thus leading to the differences of catalytic performances. According to the XRD and XPS results, we can see that the increment of calcination temperature led to the gradual coverage of niobium oxide species on the surface, indicating that the interaction between the two kinds of metal oxides got weakened. When the calcination temperature was 700 °C, the surface niobium oxide species even got crystallized. Our previous study[8] has proposed that the surface active oxygen linked to cerium species accounted mainly for the redox ability of the Ce-Nb binary oxide catalyst and niobium oxide species mainly for acidic properties. Therefore the coverage of niobium oxide species on the surface resulted in the enhancement of NH_3 adsorption but reduced the redox ability. The NH_3-TPD (see supporting information) and H_2-TPR results further confirmed this claim.Using the same method mentioned above, we calculated the ratio of $C_{L\text{-}H}/(C_{E\text{-}R}+ C_{L\text{-}H})$ at 200 °C over the catalysts

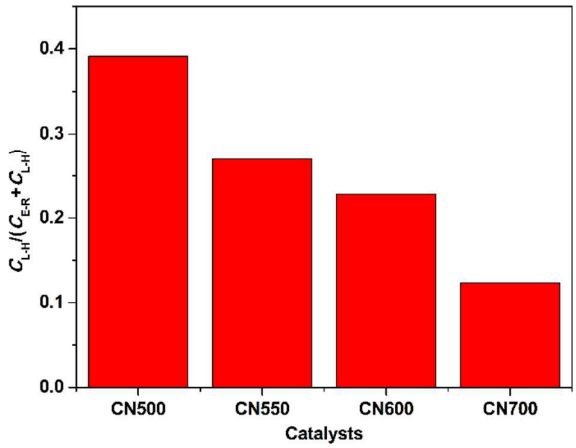

calcined at different temperatures. The result is

Fig. 9. Contribution of the Langmuir-Hinshelwood mechanism to the SCR reaction at 200 °C over Ce-Nb oxide catalysts with different calcination temperatures. Reaction condition: [NH_3]=[NO]=500 ppm, [O_2]=5 %, total flow rate=200 mL min^{-1}, catalyst mass=0.02 g, GHSV=600, 000 mL g^{-1} h^{-1}.

shown in Fig. 9. We can easily find that the contribution of L-H mechanism became less important when the catalyst calcined at higher temperatures. As discussed above, NO_2 and monodentate nitrate were the main reactive ad-NO_x species. Combining the result of NO+O_2 adsorption over the four catalysts in Fig. 6, we can see that both NO_2 and monodentate nitrate could form on the catalyst CN500, only NO_2 on CN550 and CN600, and only the relatively inert nitrate species on CN700. Considering the capability of NO oxidation, we can also observe that the NO conversion followed the order: CN500 > CN550 > CN600 >CN700, as shown in Fig. 4. Meanwhile, in Fig. 1, the catalysts calcined at lower temperatures presented lower NO conversions at temperatures higher than 400 °C. This is also the result of the differences in redox properties since the decline of NO conversion is due to the overoxidation of NH_3. These results match well with each other, indicating that the differences of ad-NO_x species and redox properties resulted in the difference of the contribution of L-H mechanism to the reaction as well as the high-temperature NO conversion.

Conclusions

By simply altering the calcination temperature, we successfully prepared the Ce-Nb binary oxide catalysts with different surface composition, and then identified the reactive species for the SCR reaction as well as calculating each contribution of Eley–Rideal mechanism and Langmuir–Hinshelwood

mechanism to the reaction. Some conclusions can be drawn as follows:

(1) The reaction over Ce-Nb binary oxide catalyst could proceed through both Eley–Rideal mechanism and Langmuir–Hinshelwood mechanism. As for the E-R mechanism, Lewis acidity was thought to be more catalytically important. NO_2 and monodentate nitrate were considered to be the reactive species in the L-H mechanism. With the increase of reaction temperature, the contribution of L-H mechanism to the reaction decreased.

(2) With the increase of calcination temperature, cerium oxide and niobium oxide got better crystallized and niobium oxide species gradually covered the catalyst surface, weakening the interaction of the two oxides. This enhanced the capability of NH3 adsorption but reduced the redox properties of the catalyst, leading to the decline of the contribution of L-H mechanism to the reaction and the shift of operation temperature window towards higher temperatures.

Acknowledgements

The authors gratefully acknowledge the financial support from the National Natural Science Foundation of China (No. 21325731 and 51125025).

References

1 G. Busca, L. Lietti, G. Ramis and F. Berti, *Appl. Catal. B-Environ.*, 1998, **18**, 1-36.
2 J. P. Dunn, H. G. Stenger and I. E. Wachs, *J. Catal.*, 1999, **181**, 233-243.
3 M. Yates, J. A. Martin, M. A. Martin-Luengo, S. Suarez and J. Blanco, *Catal. Today*, 2005, **107-08**, 120-125.
4 X. Gao, Y. Jiang, Y. C. Fu, Y. Zhong, Z. Y. Luo and K. F. Cen, *Catal. Commun.*, 2009, **11**, 465-469.
5 W. P. Shan, F. D. Liu, H. He, X. Y. Shi and C. B. Zhang, *Chem. Commun.*, 2011, **47**, 8046-8048.
6 M. Casapu, A. Bernhard, D. Peitz, M. Mehring, M. Elsener and O. Kroecher, *Appl. Catal. B-Environ.*, 2011, **103**, 79-84.
7 Z. R. Ma, D. Weng, X. D. Wu, Z. C. Si and B. Wang, *Catal. Commun.*, 2012, **27**, 97-100.
8 R. Qu, X. Gao, K. Cen and J. Li, *Appl. Catal. B-Environ.*, 2013, **142-143**, 290-297.
9 F. Kapteijn, L. Singoredjo, M. Vandriel, A. Andreini, J. A. Moulijn, G. Ramis and G. Busca, *J. Catal.*, 1994, **150**, 105-116.
10 F. D. Liu, H. He, C. B. Zhang, W. P. Shan and X. Y. Shi, *Catal. Today*, 2011, **175**, 18-25.
11 G. Ramis, L. Yi, G. Busca, M. Turco, E. Kotur and R. J. Willey, *J. Catal.*, 1995, **157**, 523-535.
12 L. Chen, J. Li and M. Ge, *Environ. Sci. Technol.*, 2010, **44**, 9590-9596.
13 N. Y. Topsoe, *Science*, 1994, **265**, 1217-1219.
14 A. Trovarelli, *Catal. Rev.*, 1996, **38**, 439-520.
15 K. I. Hadjiivanov, *Catal. Rev.*, 2000, **42**, 71-144.
16 W. S. Kijlstra, D. S. Brands, E. K. Poels and A. Bliek, *J. Catal.*, 1997, **171**, 208-218.
17 Z. Liu, S. Zhang, J. Li and L. Ma, *Appl. Catal. B-Environ.*, 2014, **144**, 90-95.
18 S. Yang, Y. Guo, H. Chang, L. Ma, Y. Peng, Z. Qu, N. Yan, C. Wang and J. Li, *Appl. Catal. B-Environ.*, 2013, **136-137**, 19-28.
19 R. Q. Long and R. T. Yang, *J. Catal.*, 2000, **190**, 22-31.
20 G. Ramis, G. Busca, F. Bregani and P. Forzatti, *Appl. Catal.*, 1990, **64**, 259-278.
21 M. Devadas, O. Kr°Cher, M. Elsener, A. Wokaun, N. Soger, M. Pfeifer, Y. Demel and L. Mussmann, *Appl. Catal. B-Environ.*, 2006, **67**, 187-196.
22 S. Yang, Y. Liao, S. Xiong, F. Qi, H. Dang, X. Xiao and J. Li, *J. Phys. Chem. C*, 2014, **118**, 21500-21508.
23 C. Ciardelli, I. Nova, E. Tronconi, D. Chatterjee and B. Bandl-Konrad, *Chem. Commun.*, 2004, 2718-2719.
24 P. Forzatti, I. Nova and E. Tronconi, *Angew. Chem.-Int. Ed.*, 2009, **48**, 8366-8368.
25 S. J. Yang, C. Z. Wang, J. H. Li, N. Q. Yan, L. Ma and H. Z. Chang, *Appl. Catal. B-Environ.*, 2011, **110**, 71-80.

Graphical Abstract